analytical chemistry

TECHNICAL NOTE

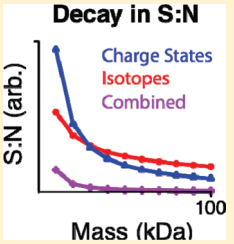
pubs.acs.org/ac

On the Scalability and Requirements of Whole Protein Mass Spectrometry

Philip D. Compton,[†,§] Leonid Zamdborg,[∥] Paul M. Thomas,[‡,§] and Neil L. Kelleher*[,†,‡,§]

[†]Department of Chemistry, [‡]Department of Molecular Biosciences, and [§]The Chemistry of Life Processes Institute, Northwestern University, Evanston, Illinois 60208, United States, and [∥]College of Medicine, University of Illinois at Urbana-Champaign, Urbana, Illinois 61801, United States

ABSTRACT: Top-down proteomics has improved over the past decade despite the significant challenges presented by the analysis of large protein ions. Here, the detection of these high mass species by electrospray-based mass spectrometry (MS) is examined from a theoretical perspective to understand the mass-dependent increases in the number of charge states, isotopic peaks, and interfering species present in typical protein mass spectra. Integrating these effects into a quantitative model captures the reduced ability to detect species over 25 kDa with the speed and sensitivity characteristic of proteomics based on <3 kDa peptide ions. The model quantifies the challenge that top-down proteomics faces with respect to current MS instrumentation and projects that depletion of ^{13}C and ^{15}N isotopes can improve detection at high mass by only <2-fold at 100 kDa whereas the effect is up to 5-fold at 10 kDa. Further, we find that supercharging electrosprayed proteins to the point of producing <5 charge states at high mass would improve detection by more than 20-fold.



In recent years, mass spectrometry-based proteomics for the analysis of whole protein molecules (i.e., no proteolysis) has realized major improvements in the number of identifications and characterizations resulting from a single liquid chromatography−mass spectrometry (LC−MS) run.[1,2] Front-end separations,[1,3−7] back-end computational tools,[8,9] and more advanced instrumentation[4] have been largely responsible for these improvements. In our laboratory, mass spectrometric instrumentation now stands as a major barrier to further advancing top-down methodologies. Here, we study how the challenge presented by electrosprayed protein ions scales with molecular weight and extrapolate our findings to prioritize the research directions that would be most likely to result in improvements of proteome coverage for top-down proteomics of complex mixtures.

Mass spectrometers are all limited to varying extents by the number of charges that can be analyzed simultaneously. As protein (peptide) masses increase, the number of channels among which this "pool" of charge is split also increases. The major channels are a result of an increased number of charge states (from electrospray ionization, ESI) as well as heavy isotopes at higher precursor mass. Further, the potential for interfering species as well as solvent adduction also increases with mass. All of these channels split the fixed number of charges present in a single scan and hinder detection at high mass.

High mass species, even if detected, may still suffer when analyzed by common data reduction algorithms. In nearly all cases, data is analyzed via the use of THRASH[10] or deconvolution.[11−13] Analysis of resolved isotopic distributions of intact or fragment ions to <1 Da accuracy relies on a close match between the experimental and theoretical data.[14,15] For small molecules, this condition is easily met not only because the charge pool is split by so few species but also because the charge states are low. Charge is drawn from the charge "pool" in quantized amounts that correspond to the charge state of the species being populated. If the charge pool is sufficiently split and the charge states of the species present in the spectrum are sufficiently high, single ions become visible as quantization in the intensities of species present in the spectrum. This quantization may result in large deviations of observed peak intensities from ideal isotopic distributions in a single scan, rendering algorithms such as THRASH susceptible to discontinuous errors (integers of 1 Da) or even unable to assign mass values reliably. Thus, averaging of spectra or summing of transients becomes necessary for mass assignment to <1 Da and robust protein identification.

Top-down proteomics typically utilizes high-resolution instrumentation to make protein/peptide identifications from an accurate precursor mass coupled with isotopically resolved fragment ions. In general, this limits top-down proteomics to time-of-flight (TOF) and Fourier transform-based (FT) instruments. As Hofstadler et al. demonstrated, isotopes generate beat patterns in the transients of FT-based instruments.[16] The increasing number of isotopes present at higher mass results in the isotopic beats becoming more narrow and spaced further apart in the time domain. Thus, these species are fundamentally more difficult to detect in FT-based instruments. TOF instrumentation relies on microchannel plate (MCP) or secondary emission multipliers (SEM) coupled to analog to digital converters (ADC) or time to digital converters (TDC). These detection strategies are limited by how quickly the detection system can recover from the previous detection event and by loss of linearity in detection efficiency at high mass.[17] Thus, while

Received: April 27, 2011
Accepted: July 11, 2011
Published: July 11, 2011

 © 2011 American Chemical Society

TOF instrumentation is not limited by space charge considerations, the number of ions that may be analyzed simultaneously is still limited, making high mass species more difficult to detect. Although these challenges will not be examined here, they are worth noting.

To our knowledge, there has been little done in the way of an integrated, quantitative treatment of the factors affecting signal-to-noise values in mass spectrometry of multiply charged protein ions. We therefore constructed a model that describes the reduction in signal-to-noise with increasing mass to both describe the challenges that instrumentation for top-down proteomics faces and direct future research. The model derived here relies on one central concept: a fixed number of charges are used during a single scan in a trapping instrument (i.e., QLT, ICR, Orbitrap). Therefore, the channels among which this charge is distributed must be considered.

EXPERIMENTAL SECTION

Isotopic Distributions and S:N Calculation. The algorithm described by Rockwood et al. was used to generate theoretical isotopic distributions for species ranging from 10 to 100 kDa.[18] The isotopic distributions were truncated where the theoretical relative abundance of isotopic peaks fell below 1×10^{-4}%. The distributions were then scaled to the most abundant isotope and the contribution from the most abundant isotope to the sum calculated. This percentage was compared to the number of charges specified for a scan and then converted to S:N by a relationship between S:N and number of charges. This process was then repeated for each isotopic depletion level following modification of the algorithm to allow calculation of isotopic distributions under depleted conditions. The depleted conditions used were natural; 99.5% ^{12}C; 99.9% ^{12}C; 99.9% ^{12}C 99.9% ^{14}N; 99.95% ^{12}C; 99.95% ^{12}C 99.95% ^{14}N; 99.99% ^{12}C 99.95% ^{14}N.

Sample Preparation and Mass Spectrometry. Solutions of ubiquitin (8.6 kDa), cytochrome C (12.3 kDa), myoglobin (16.9 kDa), carbonic anhydrase (29.0 kDa), and enolase (46.6 kDa) (5 pmol/μL) in 40% acetonitrile with 0.1% acetic acid were directly infused at 4.75 μL/min on a Q Exactive benchtop mass spectrometer (Thermo Fisher Scientific, Bremen, Germany) with 3.2 kV spray voltage, capillary temperature of 320 °C, 4 units of sheath gas flow, and no auxiliary gas flow. The instrument was operated with an S-lens value of 55 and at a resolution setting of 1 500 (at m/z 400). All reagents were purchased from Sigma-Aldrich (St. Louis, MO) and used without further purification.

RESULTS

Effect of Isotopic Peak Distributions. The contribution of heavy isotopes to the top-down measurement challenge can be dealt with entirely from isotope statistics. With the utilization of averagine,[15] theoretical isotopic distributions can be calculated for any precursor mass as well as any isotopic depletion level. If a fixed number of charges are then distributed among the peaks in the distribution, the quantity of charge present in the most abundant isotope for different masses or different depletion levels can be used as a measure of the relative signal that would be observed in a mass spectrometer. As a means of anchoring these relative values, a relationship between S:N and the number of charges present in a peak must be determined. While this relationship will not be explored here, Limbach et al. determined this experimentally for a 3 T Fourier transform ion cyclotron resonance (FTICR) mass spectrometer.[19] This method assumes only thermal noise is present during detection. Subsequently, Makarov et al. utilized this method to determine the thermal noise caused by the amplifier of an orbitrap to be equivalent to 20 charges. However, the relationship determined by Limbach et al. provides a more conservative estimate of sensitivity for the purposes of this study. Thus, the S:N ratio may be related to the number of charges by the expression:

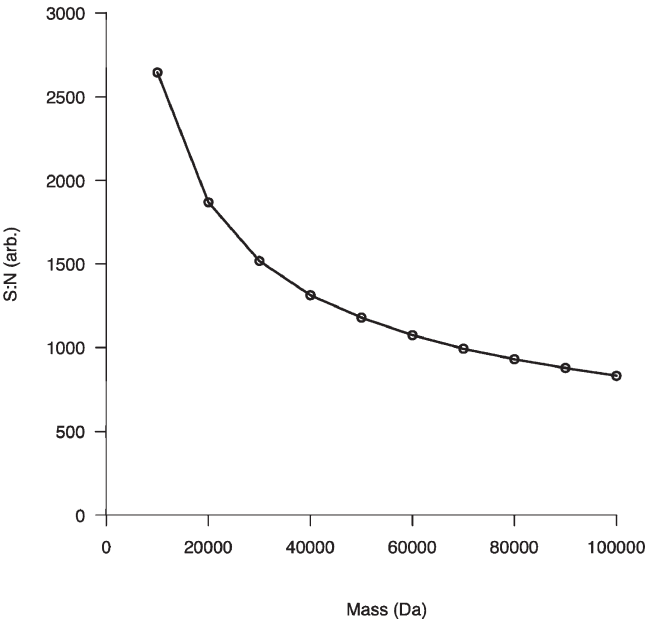


Figure 1. Reduction in S:N for a single isotopic distribution populated by 1 million charges as a function of increasing protein mass. Ions were assumed to have a 1+ charge state to eliminate contributions from charge state distributions created by ESI.

$$numberofcharges = 59(S:N) \quad (1)$$

With utilization of this relationship, the number of charges present in the most abundant isotope may be expressed as S:N. Thus, the relationship between protein mass and S:N for any number of charges may be derived. This was performed for 1 million charges, and the result is shown in Figure 1 below.

The reduction in S:N due to the presence of heavy isotopes of carbon, hydrogen, oxygen, nitrogen, and sulfur follows the relationship:

$$S:N \propto \frac{1}{\sqrt{mass}} \quad (2)$$

This behavior is expected. At higher mass, the S:N reducing effect of heavy isotopes becomes less dramatic because the additional isotopes contribute less to the total ion current than at low mass. This relationship shows a greater than 4-fold reduction in S:N from a 1 kDa to a 20 kDa species simply from the addition of isotopic peaks with increasing mass. It should be noted that, despite the negative effects on S:N, isotopic distributions at high mass have been considered for their possible analytical utility previously.[20]

With utilization of a similar process, the improvement in S:N as a function of ^{13}C, ^{15}N double isotopic depletion[21,22] can be elucidated. Figure 2 demonstrates that at extreme ^{13}C and ^{15}N

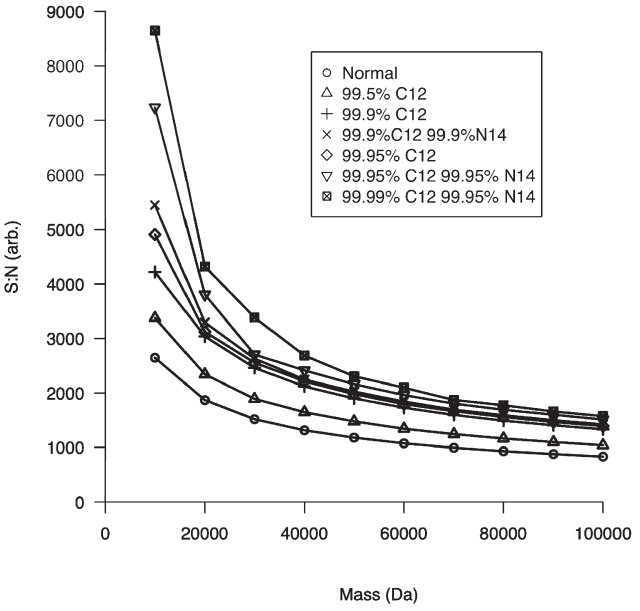


Figure 2. Reduction in S:N as a function of increasing mass at various isotopic depletion levels for a single isotopic distribution.

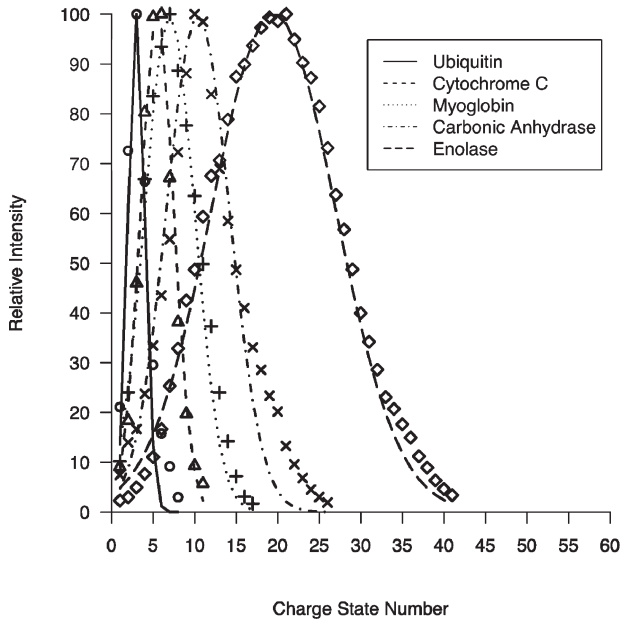


Figure 3. Experimental charge state distributions for proteins ranging from 8.6 to 47 kDa fit by Gaussian distributions.

depletion levels, the S:N at 10 kDa is expected to increase by a factor of 3. However, this gain is reduced to a factor of ~2 at 100 kDa. This surprising result can be understood by considering how isotopic distributions differ for 10 vs 100 kDa species. At lower masses, a normal isotopic distribution contains relatively few components when compared to a distribution at higher mass. When the depletion level is increased, the heaviest isotopes in the distribution contribute their intensity to the remaining isotopes in the distribution. Therefore, at higher masses, the charge "depleted" from the heaviest isotopes still has many channels to be split among when compared to the equivalent depletion at lower masses, resulting in a larger increase in signal-to-noise for lower masses.

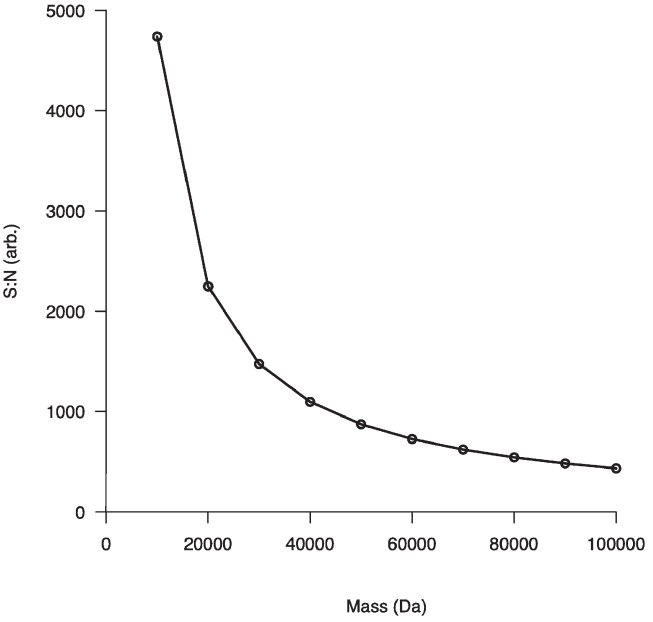


Figure 4. Decay in S:N as a function of increasing mass resulting from the increasing number of charge states observed for electrosprayed protein ions.

Effect of Charge State Distributions. Charge states resulting from ESI also serve to split ion current in a mass spectrometer. The number of charge states and their distribution as a function of mass is dependent on many factors. Solvent polarity, pH, ambient pressure, supercharging additives, and other parameters can alter charge state distributions.[23,24] Therefore, the relationships between precursor mass, number of charge states, and the distribution of charge state intensities must be determined experimentally for prototypical examples.[25] In this work, proteins from 8.6 kDa up to 47 kDa were used to model the evolution of charge state parameters as a function of mass. Figure 3 contains experimental charge state distributions normalized to the most intense charge state. The charge states were numbered in order of appearance (the highest observed charge state was labeled 1, the next 2, etc.) to eliminate the $1/z$ spacing of a standard charge state distribution. Each distribution was then fit by a simple Gaussian of the form:

$$z = e^{\left(\frac{-(n-\mu)^2}{2\sigma^2}\right)} \tag{3}$$

where n is the charge state number, μ is the average charge state, and σ is the standard deviation of the charge state distribution. The number of charge states as well as the mean and standard deviation of the Gaussian as a function of mass can then be derived, allowing the calculation of a theoretical charge state distribution for any precursor mass. The following expression is the result of this model:

$$chargestate = e^{\left(\frac{-(n-4.12\times10^{-4}(mass)-297)^2}{2(1.59\times10^{-4}(mass)-.153)^2}\right)}$$
$$for\ 0 < n < \lfloor 8.64 \times 10^{-4}(mass) + 1 \rfloor \tag{4}$$

Charge state distributions can be treated similarly to isotopic distributions. A fixed number of charges can be distributed among the peaks in the distribution based on relative intensity,

dx.doi.org/10.1021/ac2010795 |Anal. Chem. 2011, 83, 6868–6874

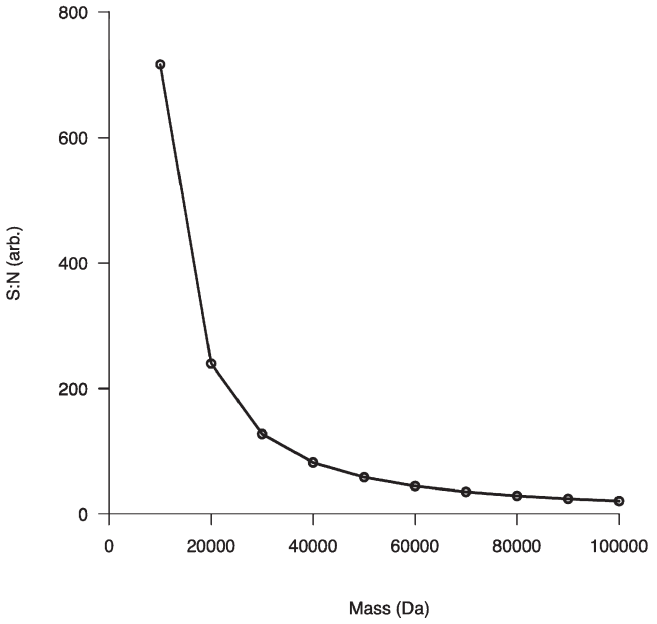


Figure 5. Combined effect of isotopes and charge states on S:N as a function of protein mass.

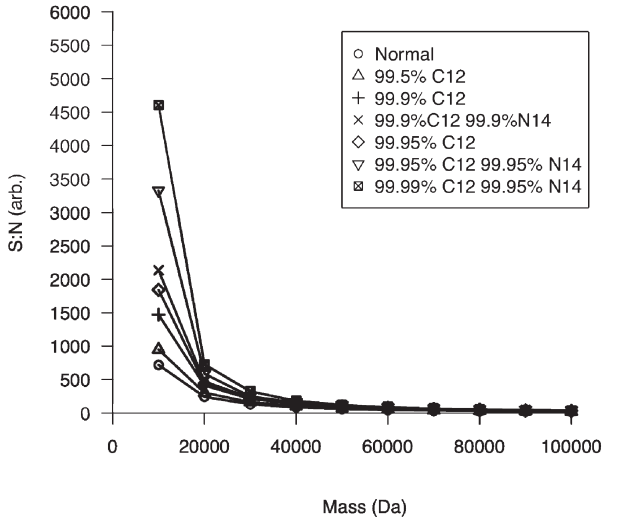


Figure 6. Effect of isotopic depletion when considered with charge state distributions.

enabling the projection of S:N decrease for proteins of all mass values. The model used here is linear over the range of proteins used to derive it. However, by analogy with isotopic effects, one would expect the S:N dependence on charge states as a function of mass to evolve with a dependency like that observed in eq 2. This relationship is simply not seen within the mass range examined because the rate of addition of charge states as a function of mass is much lower when compared to the analogous isotopic behavior. Figure 4 was generated by distributing a target number of charges among the peaks in the predicted charge state distribution as singly charged ions. Again, this was done to eliminate any bias caused by charge quantization. By comparing Figures 1 and 4, it is evident that isotopic effects are more dominant at low mass whereas charge states begin to have a greater effect on S:N over 30 kDa.

There are now several examples of "supercharging" in the literature.[26−30] While the results of these papers are encouraging, the level of supercharging accomplished is not enough to drastically impact detection of high mass species and, in some cases, overall signal is diminished by the supercharging additives. However, extreme supercharging holds the promise of large impacts on the analysis of high mass protein ions. From Figure 4, even if the charge state distribution present for a 10 kDa protein could be accomplished at 100 kDa, the benefit in S:N is ∼10-fold assuming no overall loss in signal. If the charge state envelope could be further reduced to 4−5 charge states, the gains in S:N would be ∼20-fold at 100 kDa. This is based on the combined model considering both isotopes and charge states where the number of charge states was limited to 5 instead of the predicted number of 86 at 100 kDa.

Combined Effects of Isotopes and Charge States. With the use of the expressions for charge states and isotopes, the two effects may be combined to demonstrate the overall performance of an analysis as a function of precursor mass. The intensities determined from the charge state distribution can be used to scale the corresponding isotopic distributions. Then, the charges can be distributed among all peaks. The most abundant isotope in the most abundant charge state then defines the S:N of the scan. Through the relation in eq 1, the S:N may be expressed as a function of precursor mass.

Figure 5 may be generated via the evaluation of the following expression:

$$\mathrm{S:N} = \left\{ \frac{1}{\sum_{n=1}^{n=8.62\times10^{-4}(mass)+1} \left(.0647(mass)^{1/2} \exp\left[\frac{-(n - 4.12\times10^{-4}(mass) - .297)^2}{2(1.59\times10^{-4}(mass) - .153)^2} \right] \right)} \right\} \left(\frac{target}{sensitivity} \right) \quad (5)$$

Equation 5 is an empirical expression relating the number of charges utilized in a scan (target) and the sensitivity of the instrument's detector (see eq 1) to the S:N as a function of mass (in daltons). This expression is valid for normal isotopic abundances and standard micro-ESI spray conditions from 10 to 100 kDa. The upper bound of the sum is to be rounded to the nearest integer. Within the sum, the expression for the charge state model is again visible in eq 4. It is multiplied by the isotopic model and then summed. Essentially, this is scaling the combined intensities of the isotopic distributions by the relative intensity of each charge state then summing over the charge states in the distribution. Since both the charge state and isotopic models are normalized to one, the peak defining the S:N of the scan will have a relative abundance of one. Thus, the inverse of the sum is the percent of the total ion current present in the base peak. Modifying this value by the target value and the sensitivity of

dx.doi.org/10.1021/ac2010795 |*Anal. Chem.* 2011, 83, 6868–6874

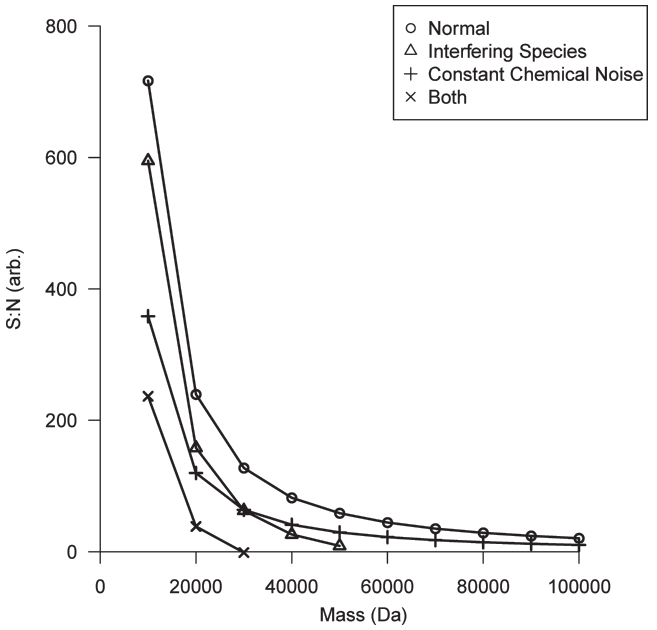


Figure 7. Contribution of various types of chemical noise to the reduction in S:N as a function of precursor mass.

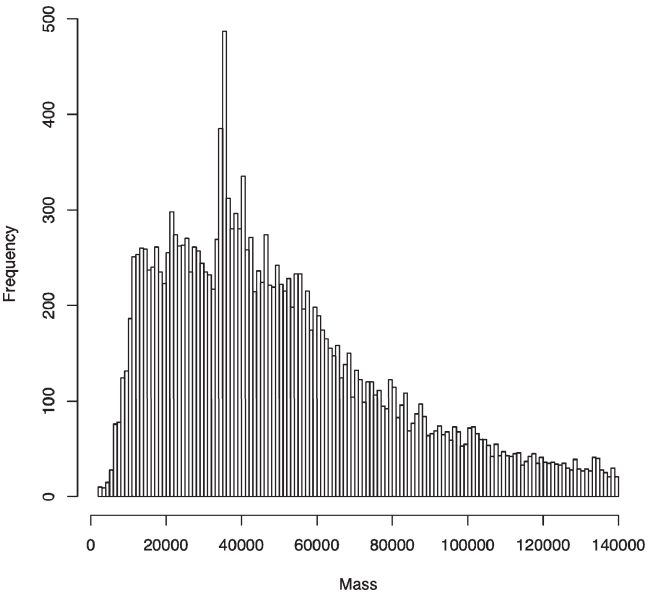


Figure 8. Histogram of protein sizes in the human proteome. The plot was created using 18 852 entries for *Homo sapiens* using the Uniprot Knowledgebase released on April 4, 2011, and the bin size is 1 000 Da.

the instrument then results in the S:N for a particular mass. With more complete models for isotopic depletion and ESI charge state distributions, much of the empirical nature of this expression can be eliminated.

The commonality in all of these graphs is the marked reduction in S:N that occurs around 20−30 kDa. Despite this, Figure 5 indicates that even species as high in mass as 100 kDa should theoretically be detectable at a S:N of ∼20 in the absence of chemical noise. Thus, chemical noise further contributes to a loss in S:N.

The effects of isotopic depletion within the combined model may also be explored. Figure 6 demonstrates the reduction in S:N as a function of mass for various isotopic depletion levels when considering charge states as well. Here, the statement that isotopic effects play a more dominant role at low mass whereas charge state effects reduce S:N more greatly at high mass is again demonstrated. For lower masses, extreme isotopic depletion provides even more benefit to S:N when considered in the context of ESI generated charge states. However, when moving to high mass, this benefit is again lost when charge state effects begin to dominate.

Effect of Chemical Noise. The topic of chemical noise is very complex and must be simplified to allow modeling. As a first approximation, chemical noise can be divided into two categories. Given a totally pure protein, multimers, solvent adducts, and unintended source fragmentation may all contribute to chemical noise. To this noise is added the complexity of biological heterogeneity. Multiply charged adduct ions,[31,32] noncovalent multimers,[33,34] and interfering species all compete with the protein of interest for charge. Here we assume this type of noise to be mass dependent. The identity of the second type of noise is related to solvent and analyte clustering with cations or anions present in the electrospray solution.[35] This noise is ever-present and fairly constant during an analysis. In considering how to model noise, it is necessary to note that the chemical noise essentially removes an amount of charge from the initial charge pool. Therefore, a simple linear reduction in the initial charge pool may be used to align theory with experiment. The *y*-int would then be the reduction in the charge pool from the constant chemical noise, and the slope would be the linear reduction due to the charge contained in adducted and interfering species.

Figure 7 contains the S:N curves resulting from various types of noise. For the constant chemical noise, 50% of the target value was arbitrarily assigned to noise and the curve regenerated. Thus, the curve is simply half the magnitude of the noiseless case. The interfering species curve was generated by assuming a slope of 17 charges/dalton. This value was chosen so that, in the combined curve, proteins beyond 30 kDa were below detectable limits. This aligns with the authors' experience with top-down proteomics analyses. Following the subtraction of this charge from the target value of 1×10^6 charges at each mass, the S:N was again calculated as described previously. The same slope and intercept were used for the combined curve.

These results may be related to typical performance characteristics of ICR instrumentation. If one assumes that, during a typical online LC−MS experiment, one million charges results in a S:N of ∼200−400 in a 7 T FTICR mass spectrometer for ubiquitin (8.6 kDa), then by examination of Figure 7, it becomes apparent that chemical noise is severely limited to detection at high mass. If the constant chemical noise is adjusted such that the predicted S:N at 10 kDa is 200, species as high as 100 kDa would still have a S:N > 3. However, upon the addition of interfering species, this situation deteriorates rapidly for high mass species as evidenced by the combined curve in Figure 7. While the depth of knowledge about the nature and properties of chemical noise makes a rigorous analytical treatment difficult, the argument presented here is sufficient to demonstrate the effects of chemical noise on detection at high mass.

A complete treatment of tandem MS is beyond the scope of this manuscript, but fragment ions will be governed in a similar manner as the effect resulting from additional isotopes. Increased precursor mass also results in more fragmentation channels. Again, the charge "pool" will be split among all fragment ions

present. Further, if charge reduction or neutral loss become dominant channels, the amount of charge present in the fragment ions may be greatly reduced due to the charge that remains in these species. Thus, tandem MS presents yet another challenge to top down proteomics.

From the treatments above, one can see that current instruments should be able to provide high-quality MS1 spectra on proteins up to 25 kDa. However, above 25 kDa, spectral averaging becomes necessary due to charge quantization and chemical noise. Also, it is shown here that isotopic depletion by 13C, 15N-double depletion[21] improves signal acquisition by a factor of 5 below 40 kDa and a factor of <2 in the 50−80 kDa regime when considered with charge state distributions.

The relevance of these findings to biological mass spectrometry can be found in the distribution of the number of proteins expressed vs mass in the human proteome. Figure 8 depicts this distribution by plotting all human proteins <140 kDa in the UniProt Knowledgebase as a histogram. Surely, modifications such as ubiquitinylation, glycosylation, sumoylation, and neddylation will shift this distribution higher, while endogenous proteolysis will shift it lower. However, it is apparent that the single scan detection limit of ∼25 kDa for isotopic resolved spectra using 1×10^6 charges in a 7 T FTICR mass spectrometer is severely limiting in terms of whole proteome coverage during LC−MS analyses. Luckily, spectral averaging serves to increase this limit but comes at the cost of acquisition time. Thus, dynamic range is reduced in the context of online LC−MS. In fact, identifications over 25 kDa in our lab are mainly a result of utilizing spectral averaging or unit resolution for MS1 detection.

When MS instruments are constructed, the quantitative models presented here will help guide instrument specifications. The experimental requirements, in some aspects, are drastically different from bottom-up proteomics and position top down proteomics as a major frontier in the future of mass spectrometer design. While current levels of supercharging and isotopic depletion in combination can provide large improvements in S:N at high mass, instruments that can simultaneously analyze a larger population of ions would provide the greatest and most easily realized benefit to top down proteomics. In addition, separation strategies capable of eliminating or reducing interfering species will be a top priority to the future of top down mass spectrometry.

AUTHOR INFORMATION

Corresponding Author

*E-mail: n-kelleher@northwestern.edu.

ACKNOWLEDGMENT

We would like to thank Mike Senko for helpful conversations and all those who contributed to the development of top down mass spectrometry along with Northwestern University and The Chicago Biomedical Consortium with support from The Searle Funds at the Chicago Community Trust. We further acknowledge the Institute on Drug Abuse (Grant DA 026672) and the Institute for General Medical Sciences at the National Institutes of Health (Grant GM 067193-09) as well as the Division of Mathematical Sciences at the National Science Foundation (Grant 0800631), whose combined investment has made accelerated progress toward the realization of top down proteomics.

REFERENCES

(1) Lee, J. E.; Kellie, J. F.; Tran, J. C.; Tipton, J. D.; Catherman, A. D.; Thomas, H. M.; Ahlf, D. R.; Durbin, K. R.; Vellaichamy, A.; Ntai, I.; Marshall, A. G.; Kelleher, N. L. *J. Am. Soc. Mass Spectrom.* **2009**, *20*, 2183–2191.

(2) Bunger, M. K.; Cargile, B. J.; Ngunjiri, A.; Bundy, J. L.; Stephenson, J. L., Jr. *Anal. Chem.* **2008**, *80*, 1459–1467.

(3) Meng, F.; Du, Y.; Miller, L. M.; Patrie, S. M.; Robinson, D. E.; Kelleher, N. L. *Anal. Chem.* **2004**, *76*, 2852–2858.

(4) Parks, B. A.; Jiang, L.; Thomas, P. M.; Wenger, C. D.; Roth, M. J.; Boyne, M. T., 2nd; Burke, P. V.; Kwast, K. E.; Kelleher, N. L. *Anal. Chem.* **2007**, *79*, 7984–7991.

(5) Sharma, S.; Simpson, D. C.; Tolic, N.; Jaitly, N.; Mayampurath, A. M.; Smith, R. D.; Pasa-Tolic, L. *J. Proteome Res.* **2007**, *6*, 602–610.

(6) Tran, J. C.; Doucette, A. A. *Anal. Chem.* **2008**, *80*, 1568–1573.

(7) Wall, D. B.; Kachman, M. T.; Gong, S.; Hinderer, R.; Parus, S.; Misek, D. E.; Hanash, S. M.; Lubman, D. M. *Anal. Chem.* **2000**, *72*, 1099–1111.

(8) Durbin, K. R.; Tran, J. C.; Zamdborg, L.; Sweet, S. M.; Catherman, A. D.; Lee, J. E.; Li, M.; Kellie, J. F.; Kelleher, N. L. *Proteomics* **2010**, *10*, 3589–3597.

(9) Leduc, R. D.; Kelleher, N. L. In *Current Protocols in Bioinformatics*; Wiley: New York, 2007; Chapter 13, Unit 13.16.

(10) Horn, D. M.; Zubarev, R. A.; McLafferty, F. W. *J. Am. Soc. Mass Spectrom.* **2000**, *11*, 320–332.

(11) Covey, T. R.; Bonner, R. F.; Shushan, B. I.; Henion, J. *Rapid Commun. Mass Spectrom.* **1988**, *2*, 249–256.

(12) Fenn, J. B.; Mann, M.; Meng, C. K.; Wong, S. F.; Whitehouse, C. M. *Science* **1989**, *246*, 64–71.

(13) Zhang, Z.; Marshall, A. G. *J. Am. Soc. Mass Spectrom.* **1998**, *9*, 225–233.

(14) Beu, S. C.; Senko, M. W.; Quinn, J. P.; McLafferty, F. W. *J. Am. Soc. Mass Spectrom.* **1993**, *4*, 190–192.

(15) Senko, M. W.; Beu, S. C.; McLafferty, F. W. *J. Am. Soc. Mass Spectrom.* **1995**, *6*, 229–233.

(16) Hofstadler, S. A.; Bruce, J. E.; Rockwood, A. L.; Anderson, G. A.; Winger, B. E.; Smith, R. D. *Int. J. Mass Spectrom.* **1994**, *132*, 109–127.

(17) Westmacott, G.; Frank, M.; Labov, S. E.; Benner, W. H. *Rapid Commun. Mass Spectrom.* **2000**, *14*, 1854–1861.

(18) Rockwood, A. L.; Vanorden, S. L.; Smith, R. D. *Anal. Chem.* **1995**, *67*, 2699–2704.

(19) Limbach, P. A.; Grosshans, P. B.; Marshall, A. G. *Anal. Chem.* **1993**, *65*, 135–140.

(20) Yergey, J.; Heller, D.; Hansen, G.; Cotter, R. J.; Fenselau, C. *Anal. Chem.* **1983**, *55*, 353–356.

(21) Marshall, A. G.; Senko, M. W.; Li, W. Q.; Li, M.; Dillon, S.; Guan, S. H.; Logan, T. M. *J. Am. Chem. Soc.* **1997**, *119*, 433–434.

(22) Xiong, Y.; Schroeder, K.; Greenbaum, N. L.; Hendrickson, C. L.; Marshall, A. G. *Anal. Chem.* **2004**, *76*, 1804–1809.

(23) Iavarone, A. T.; Jurchen, J. C.; Williams, E. R. *J. Am. Soc. Mass Spectrom.* **2000**, *11*, 976–985.

(24) Chen, L. C.; Mandal, M. K.; Hiraoka, K. *J. Am. Soc. Mass Spectrom.* 2011, *22*, 539–544.

(25) Dobo, A.; Kaltashov, I. A. *Anal. Chem.* **2001**, *73*, 4763–4773.

(26) Iavarone, A. T.; Jurchen, J. C.; Williams, E. R. *Anal. Chem.* **2001**, *73*, 1455–1460.

(27) Loo, J. A.; Edmonds, C. G.; Udseth, H. R.; Smith, R. D. *Anal. Chem.* **1990**, *62*, 693–698.

(28) Loo, J. A.; Udseth, H. R.; Smith, R. D. *Biomed. Environ. Mass Spectrom.* **1988**, *17*, 411–414.

(29) Valeja, S. G.; Tipton, J. D.; Emmett, M. R.; Marshall, A. G. *Anal. Chem.* **2010**, *82*, 7515–7519.

(30) Sterling, H. J.; Cassou, C. A.; Trnka, M. J.; Burlingame, A. L.; Krantz, B. A.; Williams, E. R. *Phys. Chem. Chem. Phys.* **2011**, DOI: 10.1039/C1CP20277D.

(31) Gardner, M. W.; Brodbelt, J. S. *J. Am. Soc. Mass Spectrom.* **2009**, *20*, 2206–2210.
(32) Loo, J. A.; Udseth, H. R.; Smith, R. D. *Rapid Commun. Mass Spectrom.* **1988**, *2*, 207–210.
(33) Counterman, A. E.; Hilderbrand, A. E.; Barnes, C. A. S.; Clemmer, D. E. *J. Am. Soc. Mass Spectrom.* **2001**, *12*, 1020–1035.
(34) Lightwahl, K. J.; Schwartz, B. L.; Smith, R. D. *J. Am. Chem. Soc.* **1994**, *116*, 5271–5278.
(35) Cech, N. B.; Enke, C. G. *Mass Spectrom. Rev.* **2001**, *20*, 362–387.